3. Geodesy and Geodynamics. Laboratoire de Géologie de l'Ecole normale supérieure. Available at: https://www.geologie.ens.fr/en/recherche-en/equipes-en/geodynamics-and-structures/ (accessed: 12.04.2024).
4. Nahavandchi H., Soltanpour A. Improved determination of heights using a conversion surface by combining gravimetric quasi/geoid and GPS-levelling height differences. *Studia Geophysica et Geodaetica*. 2006. Vol. 50. pp. 165–180.
5. Mandrikova O. V., Solovev I. S., Zalyaev T. L. Methods of analysis of geomagnetic field variations and cosmic ray data. *Information Technologies*. 2015. Vol. 21, No. 11. pp. 849–855.
6. Stolbova A. A. Operating speed of wavelet transform algorithms. *New Information Technologies in Scientific Research : Proceedings of XXII All-Russian Conference of Students, Young Scientists and Specialists*. 2017. pp. 173–174. ID 30521218.
7. Rafiei M., Niknam T., Khooban M. H. Probabilistic electricity price forecasting by improved clonal selection algorithm and wavelet preprocessing. *Neural Computing and Applications*. 2017. Vol. 28. pp. 3889–3901.
8. Turekhanova V. B. A modern approach to the determination of quasigeoid. *Proceedings of International Conference of Students and Young Scientists — Farabi Alemi*. 2018. pp. 185–186.
9. Kadlec M. Refining gravity field parameters by residual terrain modelling. PhD Theses, Pilsen, Czech Republic : University of West Bohemia, 2011. 150 p.
10. Iophis M. A., Odintsev V. N., Blokhin D. I., Sheinin V. I. Experimental investigation of spatial periodicity of induced deformations in a rock mass. *Journal of Mining Science*. 2007. Vol. 43, No. 2. pp. 125–131.
11. Mozzi P., Fontana A., Ferrarese F., Ninfo A., Campana S. et al. The Roman City of Altinum, Venice Lagoon, from remote sensing and geophysical prospection. *Archaeological Prospection*. 2016. Vol. 23, Iss. 1. pp. 27–44
12. Karpik A. P., Kanushin V. F., Ganagina I. G., Goldobin D. N., Mazurova E. M. The study of the spectral characteristics of global models of the Earth's gravitational field obtained from the space missions CHAMP, GRACE and GOCE. *Giroskopiya i Navigatsiya*. 2014. No. 4(87). pp. 34–44.
13. Kanushin V. F., Karpik A. P., Ganagina I. G., Goldobin D. N., Kosarev N. S., et al. The study of modern global models of the gravitational field of the Earth. Novosibirsk : SSUGT, 2015. 270 p.
14. Zolotova E. V., Skogoreva R. N. Geodesy, Cadaster with Elementaries of Geoinformation Science : University Textbook. Moscow : Akademicheskiy Proekt, 2020. 532 p.
15. Thanh Ph. T., Kornienko A. Yu., Hoa Ph. T. Description of the global geoid models. *Burning Issues of Land Use and Property Management. Proceedings of All-Russian Conference with International Participation*. 2019. pp. 141–151. ID 38193336.
16. Dolgal A. S., Pugin A.V., Novikova P. N. History of the method for source-wise approximations of geopotential fields. *Izvestiya*, *Physics of the Solid Earth*. 2022. Vol. 58, No. 2. pp. 149–171.
17. Romanchak V. M. Approximation by singular wavelets. *System Analysis and Applied Information Science*. 2018. No. 2. pp. 23–28.
18. Zhurkin I. G., Neiman Yu. M. Calculation methods in geodesy. Moscow : Nedra, 1988. 304 p.
19. Kim K. B., Yun H. S., Choi H. J. Accuracy evaluation of geoid heights in the national control points of south Korea using high-degree geopotential model. *Applied Sciences*. 2020. Vol. 10, Iss. 4. ID 1466.
20. Ince E. S., Barthelmes F., Reißland S., Elger K., Förste C. et al. ICGEM — 15 years of successful collection and distribution of global gravitational models, associated services, and future plans. *Earth System Science Data*. 2019. Vol. 11, Iss. 2. pp. 647–674.
21. Sansò F., Reguzzoni M., Barzaghi R. Geodetic Heights. Switzerland : Springer Geophysics, 2019. DOI: 10.1007/978-3-030-10454-2
22. Oduyebo O. F., Ono M. N., Eteje S. O. Comparison of three gravimetric-geometric geoid models for best local geoid model of Benin City, Nigeria. *International Journal of Advanced Engineering Research and Science*. 2019. Vol. 6, Iss. 12. pp. 261–272.
23. Turekhanova V., Saliy S., Kudaibergenovet M. Application of the wavelet transformation theory in the algorithm for constructing a quasigeoid model. *Naukovyi Visnyk Natsionalnoho Hirnychoho Universytetu*. 2022. No. 4. DOI: 10.33271/nvngu/2022-4/ EM

UDC 622.831; 622,2; 622.235

***M. A. KOSYREVA**[1], Post-Graduate Student*
***V. A. EREMENKO**[1], Professor, Doctor of Engineering Sciences, prof.eremenko@gmail.com*

[1]College of Mining, National University of Science and Technology – MISIS, Moscow, Russia

NUMERICAL STRESS–STRAIN MODELING OF HONEYCOMB MINE STRUCTURES WITH VERTICAL STOPES OF CYLINDRICAL FORM

The article describes the numerical modeling results of the stress–strain behavior of a room-and-pillar stoping system in honeycomb mine design including rib pillars with their angles cut off by vertical cylindrical stopes. The factors of safety are calculated for the pillars and enclosing rock mass with the excessive stresses and displacement in rock mass. The authors present a selected variant of the numerical stress–strain modeling of rib pillar with angles cut off by vertical stopes of cylindrical form in case of cellular arrangement of the stopes for the conditions of mining at the depths of 400 and 1000 m. The numerical calculation of the critical depths for using honeycomb mine structures is presented as a case-study of geological and geotechnical conditions of the Ilets rock salt deposit. The patterns of destructive loads are obtained in numerical models at different ratios of minimal widths of pillars and diameters of stopes.

***Keywords:** Turner–Shevyakov hypothesis, numerical modeling, rib pillar, pillars with angles cut off by vertical stopes of cylindrical form, honeycomb mine structure, factor of safety, excessive stress, rock mass displacement, rock salt deposit*
***DOI:** 10.17580/em.2024.01.09*

Introduction

The scientific works [1–7] described a new geotechnical approach and the concept of an alternative convergent geotechnology for solid mineral deposits, including the Ilets rock salt deposit [2, 3, 8, 9], based on the change of the stoping front advance, i.e., transition from horizontal stoping to top-downward or bottom-upward vertical stoping in cylindrical stopes made by drilling. Calculation of the stability of rib pillars used the Turner–Shevyakov hypothesis for the conventional room-and-pillar mining systems [10–13] and for the vertical cylinder-shaped stopes with the rib pillars with their angles cut off by circles.

Table 1. Model alternatives of vertical stopes of cylindrical form, with different structural members of extraction block for Sol-Ilets Mine (dimension of model (extraction panel, block) 60×60×60 m) (see Fig. 1)

Model No.	Model volume, m^3	Horizontal area of model, m^2	Diameter (width b_s, length d_s) of stope, m	Minimum width a_p (length d_p)/ Maximum width A_p (length D_p) of pillar, m	Number of stopes in model/in row	Horizontal area of voids (stopes) in model, $S_{\Sigma Sm}$, m^2	Horizontal area of rock salt mass in pillars, $S_{\Sigma Pm}$, m^2	Width of perimeter pillar, m	Operating losses in pillars, L_{Pm}, %
1	216 000	3600	2	0.5/2.5	529/23	1661.06	1702.94	1.5	50.62
2			2	1/3	361/19	1133.54	2230.46	2	66.30
3			3	0.75/3.75	225/15	1589.625	1659.375	2.25	51.07
4			3	1.5/4.5	169/13	1193.985	2406.015	1.5	66.83
5			4	1/5	121/11	1519.760	1616.24	3	51.54
6			4	2/6	81/9	1017.360	2118.64	4	67.56
7			5	1.25/6.25	81/9	1589.625	1716.625	2.5	51.92
8			5	2.5/7.5	49/7	961.625	2063.375	5	68.21
9			6	1.5/7.5	49/7	1384.740	1531.26	4.5	52.51
10			6	3/9	36/6	1017.360	2231.64	4.5	68.69

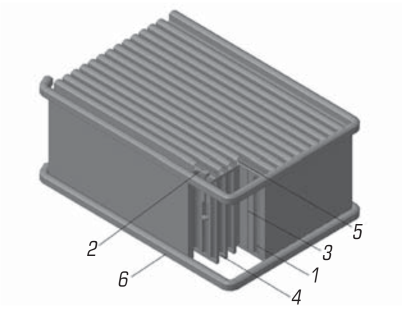

Fig. 1. 3D model of extraction block/panel mining using honeycomb mine structure with vertically arranged stopes of cylindrical form: *1* – vertical cylindrical stopes; *2* – well drilling rig; *3* – pilot bore; *4* – haulage level; *5* – drilling and ventilation level; *6* – main ring roadway

Pending the further study, the authors performed the stress–strain analysis and modeling for mine structures including vertical stopes of cylindrical form (**Fig. 1**) [2, 3, 14, 15].

The numerical calculus and analyses used AutoCAD with a Midas software for the complex 3D modeling, as well as for the study and visualization of pressure and deformations at stope boundaries and in pillars at different indexes of rock mass quality [16–21]. The stability criteria of the pillars and enclosing rock mass were: the stress σ_{max} (excessive stress $\Delta\sigma$), the factor of safety (FoS) and the displacement X.

Numerical modeling results

For the numerical modeling, the alternative designs are developed (**Table 1**) and adjusted to the mining conditions of the Ilets rock salt deposit. The extraction panel was selected to be a cubic rock salt block with the sizes L (length) × W (width) × H (height) = 60×60×60 m. The height of the block and the diameters of the stopes are selected with regard to efficient performance of drilling equipment so that to embrace the selected height of the block as the height of two levels 30 m high each. The geometrical parameters of the models and their structural members, with the area ratio of voids (vertical stopes) and rock salt, as well as the physical and mechanical properties of rock salt and the modeling conditions are described in **Tables 1–3** and in **Fig. 2**.

Table 2. Physical and mechanical properties of Ilets rock salt

Parameter	Value
Rock salt bulk volume γ, kN/m^3	20.9
Uniaxial compression strength σ_c, kN/m^2	35 000
Poisson's ratio ν	0.35
Cohesion C, kN/m^2	4500
Elastic modulus E, kN/m^2	30 000 000
Internal friction angle φ, degree	41
GSI (geological strength index)	95
Structural index *mi*	10

Table 3. Numerical modeling parameters

Parameter	Structural members and modeling conditions
Height of block, m	60
Width of block, m	60
Length of block, m	60
Stope pattern design	Square
Height of stope, m	60
Initial stress field	Lithostatic
Mining depth below ground surface, m	250–310 m 400–460 m 600–660 m 1000–1060 m
Principal stresses at the initial lithostatic stress field, kN/m^2	$\sigma_1 = \gamma H$ (vertical) $\sigma_2 = \gamma H$ (horizontal) $\sigma_3 = \gamma H$ (horizontal)

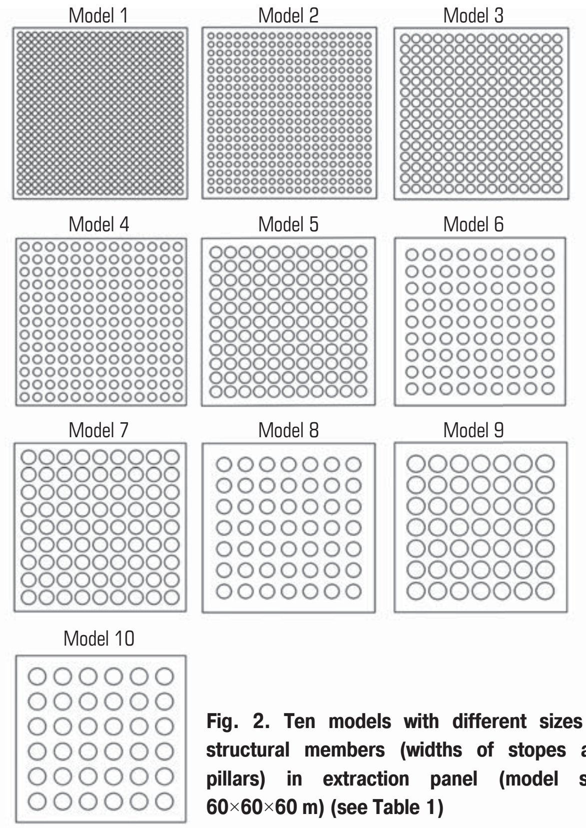

Fig. 2. Ten models with different sizes of structural members (widths of stopes and pillars) in extraction panel (model size 60×60×60 m) (see Table 1)

a

b

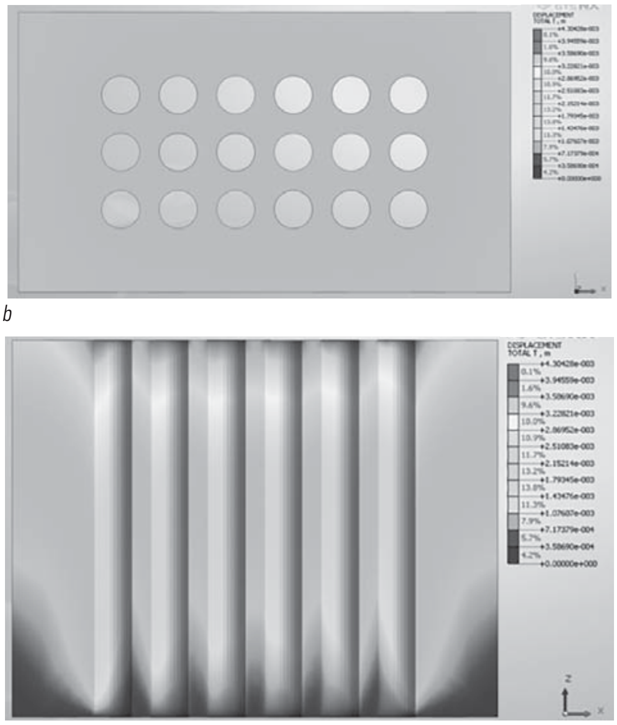

Fig. 3. Numerical modeling in Midas: stress–strain behavior of honeycomb mine structure (Table 1, Model 10) with maximal displacements in enclosing rock mass at the depth *H* = 400 m (*a* — horizontal section in the center of the block/model 60×60×60 m, *b* — vertical section). DISPLACEMENT TOTAL *T* — maximal displacements at the final calculus stage: color spectrum (displacement range) 0.000358690–0.00430428 m

a

b

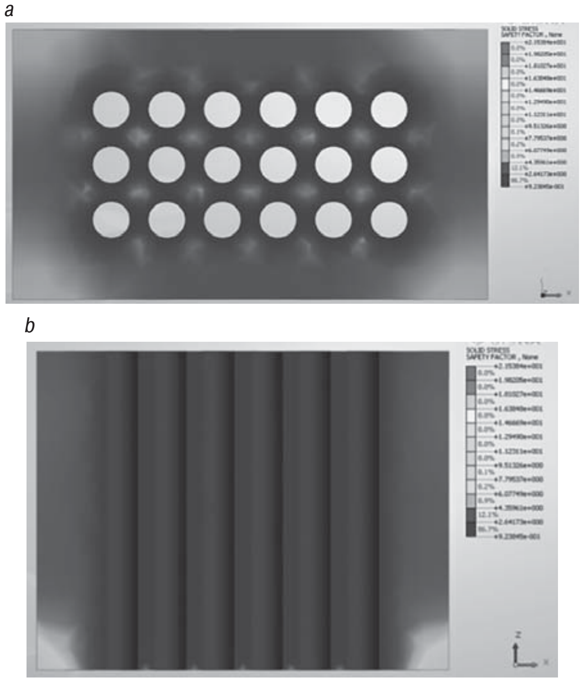

Fig. 4. Numerical modeling and stress–strain analysis in Midas for honeycomb mine structure (Table 1, Model 10) with factor of safety determined in enclosing rock mass and in pillars at the depth *H* = 1000 m (*a* — horizontal section in the center of the block/model 60×60×60 m, *b* — vertical section). SOLID STRESS SAFETY FACTOR — factor of safety at the final calculus stage: color spectrum (FoS range) 0.923845–20.15384

Table 4. Enclosing rock mass instability criterion for numerical modeling

Range of maximal displacements X*, m	Processes and events
0.000–0.075	Low probability of deformation and failure
0.076–0.140	Mean probability of deformation and failure
0.0141–0.260	Small-volume failure is probable
0.261–0.480	Average-volume failure is probable (FoS**<1.3–1.5)
0.481–>>0.65	Large-volume failure is probable (FoS**<1.2–1.3)
*Results of long-term full-scale observations **Allowable factor of safety for pillars (in mine design) in numerical analysis at high reliability of input data is assumed as FoS ≥1.5	

By way of example, **Figs. 3** and **4** depict the resultant calculations of the maximal displacements X in enclosing rock mass surrounding vertical stopes of cylindrical form in the honeycomb layout at the final calculation stage at the depth of 400 m, and the factor of safety at the depth of 1000 m, respectively. The maximal displacement in the model is X = 0.00430428 m, which conforms with the displacements from the range of low probabilities of deformation and failure (**Table 4**). The enclosing rock mass at the depth of 1000 m occurs both in stable and in transient state (FoS = 0.923845–20.15384; when FoS ≤ 1 plastic deformations are recorded and rock mass fails), which is confirmed by the high level of reliability of the model input data since the rock mass is homogenous and uniform, the physical and mechanical properties change slightly with depth, and the initial stress field is lithostatic.

Geotechnical design should use the results of numerical modeling with the highly reliable input data given that FoS ≥ 1.5. The developed graph (**Fig. 5**) allows determining critical depths of 340–470 m for the application of the honeycomb mine structures for the conditions of the Ilets rock salt deposit, with rib pillars with their corners cut off by the vertical stopes of cylindrical form when FoS ≥1.5, at different ratios of the minimum width of pillars, a_p, and diameters of stopes, $b_s : a_p = 0.5$; 0.75; 1;1.25; 1.5; 2; 2.5; 3 m conform with $b_s = 2$; 3; 2 and 4; 5; 3 and 6; 4; 5; 6 m, with possibility to increase mining depth by means of increasing the width of pillars and decreasing the height of levels [2, 3].

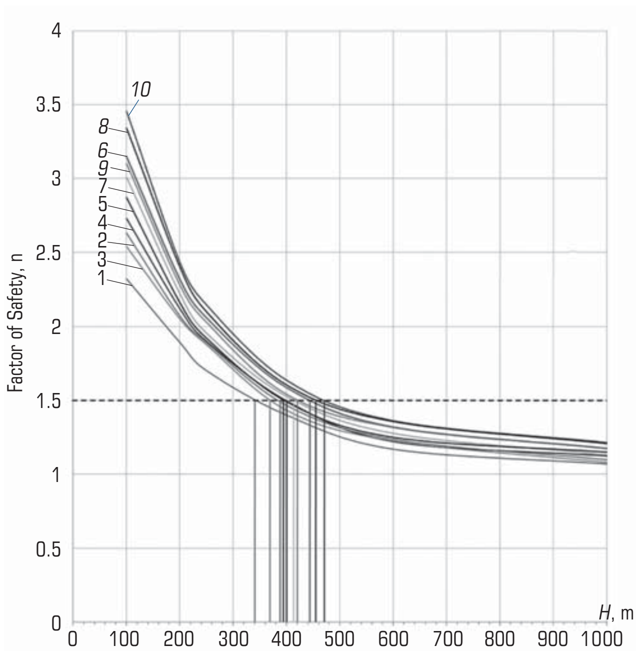

Fig. 5. Change in factor of safety in pillars, n, with depth and allowable application depths for Models Nos. 1–10. FoS ≥ 1.5 — allowable threshold of geotechnical system design at high reliability of input data of numerical model

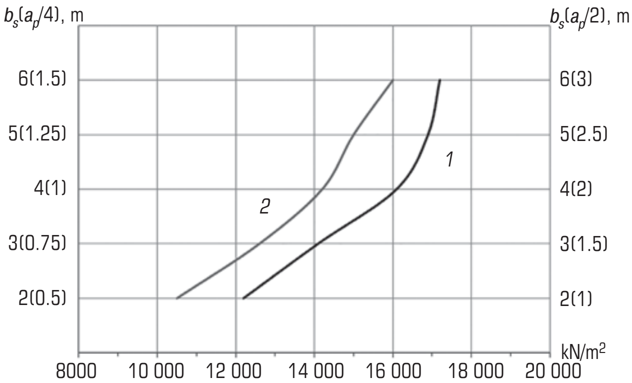

Fig. 6. Change in destructive loads (P_n, kN/m²) in numerical modeling at varied widths of stopes and pillars, b_s and a_p, respectively:
1 – pillar width is half as much as stope width; *2* – pillar width is four times smaller than stope width

Table 5. Rating of models by resistance to destructive loads at different stope and pillar width ratios (see Table 1)

Model No.	Destructive load or limit pressure P_n, kN/m²	Rating of model by load resistance from 1 (maximum stability) to 10 (minimum stability)	Stope width b_s, m	Minimum pillar width a_p, m
1	10 500	10	2	0.5
2	12 200	8	2	1
3	13 100	9	3	0.75
4	13 500	7	3	1.5
5	14 200	6	4	1
6	16 100	3	4	2
7	15 000	5	5	1.25
8	16 900	2	5	2.5
9	16 000	4	6	1.5
10	17 200	1	6	3

The study aimed to perform the stress–strain analysis in 10 numerical models with the stope diameters of 2, 3, 4, 5 and 6 m, and with the sizes of rib pillars, with angles cut-off by vertical stopes of cylindrical form, 2 and 4 times smaller than the stope widths (see Table 1, Fig. 2). The found patterns of destructive loads, or limit stresses, in the models are described in **Table 5** and in **Fig. 6**: with the increase in the stope diameters b_s at the half as much minimum pillar width a_p, and with the decrease in the pillar width from 2 to 4 times as against the stope diameter, the resistance of the enclosing rock mass and rib pillars to the limit loading decreases. At the smaller width of the pillars, the destructive loads in the models regularly decrease. These results are confirmed by the physical simulation data to be described in the other article.

Conclusions

The article describes the numerical studies on the strength of the honeycomb mine structures including vertical stopes of cylindrical form.

Within the geotechnical design, the critical depths for the honeycomb mine structure, including rib pillars with the angles cut off by the vertical cylindrical stopes are determined as a case-study of the Ilets rock salt deposit, at different ratios of the minimum widths of the pillars and diameters of the stopes. The obtained values of the critical depth are confirmed by the numerical modeling results.

The patterns of the destructive loads are obtained in the numerical models at different ratios of the minimum widths of the pillars and diameters of the stopes.

The results demonstrate the promising nature of using the honeycomb mine structures in underground mining of rock, polymineral, potassium and potassium–magnesium salts and polyhalites at high safety and efficiency.

References

1. Galchenko Yu. P., Eremenko V. A. Natural–technical systems of underground or mining using convergent technologies. Monograph. 2nd edition, extended and amended. Zakharov V. N. (Ed.). Moscow : Gornaya kngia, 2023. 288 p.
2. Eremenko V. A., Vinnikov V. A., Pugach A. S., Kosyreva M. A. Substantiation of rib pillar sizes for rock salt mining in vertical cylindrical stopes arranged at the nodes of regular triangular pattern. *Eurasian Mining*. 2023. No. 2. pp. 56–62.
3. Eremenko V. A., Vinnikov V. A., Pugach A. S., Kosyreva M. A. Substantiation of rib pillar sizes for rock salt mining in vertical cylindrical stopes. *Gornyi Zhurnal*. 2024. No. 1. pp. 29–38.
4. Sidorov D. V., Ponomarenko T. V. Estimation methodology for geodynamic behavior of nature-and-technology systems in implementation of mineral mining projects. *Gornyi Zhurnal*. 2020. No. 1. pp. 49–52.
5. Trubetskoy K. N., Galchenko Yu. P. Nature-like geotechnology for integrated subsoil use : Problems and prospects. Moscow : Nauchtekhlitizdat, 2020. 368 p.
6. Trubetskoy K. N., Galchenko Yu. P. Geoecology of subsoil use and eco-geotechnology of mineral mining. Moscow : Nauchtekhlitizdat, 2015. 360 p.
7. Shadrin M. A., Sidorov D. V., Kornaushenko A. P., Mulev S. N. Modern geomechanical assessment of influence of rockbursts in tectonic areas on mine stability in the North Urals Bauxite Mine. *Gornyi Zhurnal*. 2022. No. 1. pp. 4–11.
8. Dzens-Litovskiy A. I. Geological and hydrogeological observation procedure for rock salt mines. Leningrad, 1945. 171 p.
9. Dzens-Litovskiy A. I., Karegunova G. V., Orlyankin O. M., Mazherova E. I. The Ilets rock salt deposit and its hydrogeology. Orenburg, 1939. 358 p.
10. Shevyakov L. D. Calculation of strong dimension and deformation of support pillar. Moscow : AN SSSR, 1941, No. 7–9.
11. Shevyakov L. D. Mineral mining. Moscow : Ugletekhizdat, 1953.
12. Borsch-Komponiets V. I. Practical geomechanics of rocks. Moscow : Gornaya kniga, 2013. 322 p.
13. Gulevich G. E. Rational arrangement and optimal sizes of support pillars in room-and-pillar mining. Moscow : OBNTI Giprotsvetmet, 1958.
14. Eremenko V. A., Kosyreva M. A., Vysotin N. G., Khazhy-ylai Ch. V. Geomechanical justification of room-and-pillar dimensions for rock salt and polymineral salt mining. *Gornyi Zhurnal*. 2021. No. 1. pp. 37–43.
15. Eremenko V. A., Myaskov A. V., Galchenko Yu. P., Romero Barrenechea Moisés Esau, Substantiation of convergent technology parameters for Ilets rock salt deposit. *Journal of Fundamental and Applied Problems of Mining Science*. 2018. Vol. 5. pp. 37–48.
16. Protosenia A. G., Verbilo P. E. Strength assessment of blocky massif with a method of numerical simulation. *Minerals and mining engineering*. 2016. No. 4. pp. 47–54.
17. Zhengzheng Xie, Nong Zhang, Xiaowei Feng, Dongxu Liang, Qun Wei. et al. Investigation on the evolution and control of surrounding rock fracture under different supporting conditions in deep roadway during excavation period. *International Journal of Rock Mechanics and Mining Sciences*. 2019. Vol. 123. ID 104122.
18. Islavath S. R., Deb D., Kumar H. Development of a roof-to-floor convergence index for longwall face using combined finite element modelling and statistical approach. *International Journal of Rock Mechanics and Mining Sciences*. 2020. Vol. 127. pp. 204–221.
19. Fei Wu, Hao Zhang, Quanle Zou. et al. Viscoelastic-plastic damage creep model for salt rock based on fractional derivative theory. *Mechanics of Materials*. 2020. Vol. 150. pp. 1–14. ID 103600.
20. Jianqiang Deng, Yaoru Liu, Qiang Yang. et al. A viscoelastic, viscoplastic, and viscodamage constitutive model of salt rock for underground energy storage cavern. *Computers and Geotechnics*. 2019. Vol. 119. ID 103288.
21. Huang Xiao Lan, Chao Yu. Studies of hard interlayer's influence on the creep deformation of salt rock cavity. *Advanced Materials Research*. 2012. Vol. 594–597. pp. 452–455. EM